

**FIG 6.** Increased penetration of foreign materials in *Flg*<sup>-/-</sup> mice. **A** and **C**, Calcein solution (Fig 6, **A**) and calcein encapsulated in liposomes (Fig 6, **C**) were topically applied to the tails of 8-week-old mice, and permeability was examined with confocal microscopy. **B** and **D**, Penetration ratio: the proportion of fluorescence that penetrated more than half of the SC. Dashed white lines, Border between the SC and SG. +/+, Wild-type mice; -/-, *Flg*<sup>-/-</sup> mice; NS, not significant.

edema and inflammation (Fig 7, **C**), indicating that *Flg*<sup>-/-</sup> mice exhibited exaggerated irritant and allergic contact dermatitis responses.

These results prompted us to evaluate protein antigen-specific humoral responses to percutaneously applied OVA. Langerhans cells have been shown to be capable of capturing protein antigens that exist outside epidermal tight junction barriers<sup>29,30</sup> and then elicit T<sub>H</sub>2 humoral responses *in vivo*.<sup>30,31</sup> Because topical application of OVA alone did not elicit a response, we repeatedly applied OVA with dibutyl phthalate, which is reported to be a T<sub>H</sub>2 adjuvant,<sup>32</sup> to the ear skin of mice and measured OVA-specific serum antibody levels. Concordant with the hapten-induced CHS results, IgG<sub>1</sub> and IgE responses to OVA were enhanced in *Flg*<sup>-/-</sup> mice (Fig 7, **D**), demonstrating exaggerated T<sub>H</sub>2 humoral responses in the absence of filaggrin. Collectively, our results suggest that alterations in the SC barrier in *Flg*<sup>-/-</sup> mice allowed penetration of irritants, haptens, and protein antigens and led to exaggerated responses in the context of irritant contact dermatitis and T<sub>H</sub>1 and T<sub>H</sub>2 immune responses.

## DISCUSSION

Filaggrin has been demonstrated to function in SC integrity as a structural protein that organizes keratin filaments.<sup>6</sup> It is also a major source of the hygroscopic amino acids in SC referred to as NMFs.<sup>8</sup> NMFs are believed to maintain SC hydration levels.<sup>8</sup> Although the biology and functions of filaggrin have been modeled through *in vitro* experiments, its *in vivo* functions have remained elusive because of the absence of mice that completely and specifically lack filaggrin. This was due to technical difficulties in generating *Flg*<sup>-/-</sup> mice, which were attributed to the tandem repeats in *Flg* and complicated gene sequencing and targeting strategies. Given the growing importance of filaggrin in the context of AD, we successfully generated *Flg*<sup>-/-</sup> mice and used these mice to explore the role of filaggrin *in vivo*.

We unexpectedly observed that loss of NMFs as a result of filaggrin deficiency did not lead to decreased SC water content.

Despite the dry appearance of their skin, *Flg*<sup>-/-</sup> mice exhibited normal SC hydration throughout their lives. It is interesting to compare *Flg*<sup>-/-</sup> mice with *ft/ma* mice, which have been reported to have spontaneous dermatitis (see Fig E2) and to display increased TEWL and loss of SC hydration,<sup>14,17</sup> which is consistent with findings in human AD (with and without *FLG* mutations).<sup>33</sup> We subsequently found that whereas TEWL and SC hydration were not impaired in *ft/ma* mice before the onset of dermatitis, TEWL increased and SC hydration decreased after these mice had dermatitis (see Fig E3 in this article's Online Repository at [www.jacionline.org](http://www.jacionline.org)). These data indicate that increased TEWL and SC water loss in *ft/ma* mice are secondary to skin inflammation. Hydration of SC *in vivo* is also reported to be maintained by several other factors, such as intercellular lamellar lipids,<sup>8</sup> and is influenced by environmental aspects, such as humidity. The relation between filaggrin and SC hydration should be interpreted carefully.

Analyses of *Flg*<sup>-/-</sup> mice clearly demonstrated the important contribution of filaggrin to keratin filament network assembly *in vivo*. Filaggrin-deficient epidermis showed immature bundles and an aberrant network of keratin filaments in upper parts of the SG and loss of the keratin pattern in the lower SC. Interlaced keratin filaments form 3-dimensional lattice-like structures that physically stabilize the corneocyte keratin framework.<sup>27</sup> Loss of this interlaced keratin pattern in *Flg*<sup>-/-</sup> epidermis led to increased susceptibility to mechanical stress. Although it was previously found that some patients with IV display normal keratin patterns,<sup>34,35</sup> this likely depends on the mutation site and the extent of filaggrin loss.<sup>36</sup>

Events accompanying barrier dysfunction, in particular enhanced penetration by antigens and subsequent sensitization, are important immunologic steps in the pathogenesis of AD. In this study, evaluation of SC permeability revealed that *Flg*<sup>-/-</sup> skin exhibited enhanced penetration of liposome-encapsulated calcein throughout the SC layer in focal areas (Fig 6, **C** and **D**). This can be attributed to increased SC fragility and premature desquamation in *Flg*<sup>-/-</sup> mice. Interestingly, however, calcein

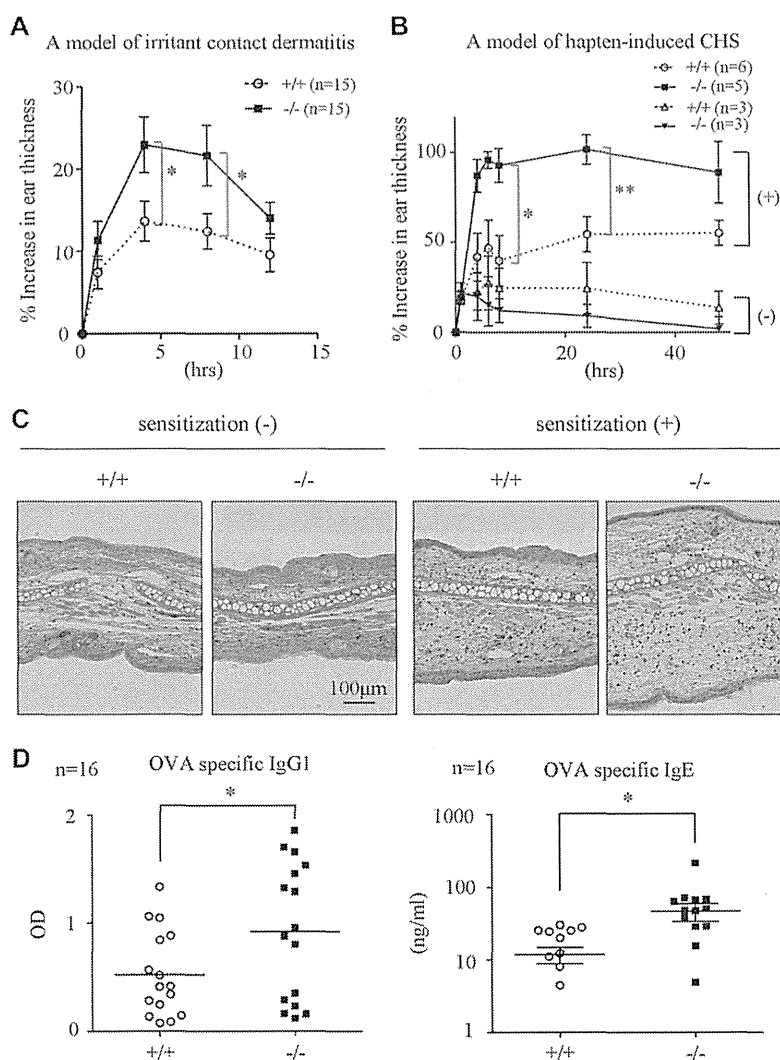


**FIG 7.** Enhanced percutaneous immune responses in *Flg*<sup>-/-</sup> mice. **A** and **B**, Percentage increase in ear thickness of mice after topical application of croton oil (Fig 7, **A**) and after DNFB challenge with (+) or without (-) sensitization (Fig 7, **B**). **C**, Histology after DNFB challenge. **D**, Systemic immune responses to repeated percutaneous application of OVA. OVA-specific serum IgG, and IgE levels were measured by using ELISA. +/+, Wild-type mice; -/-, *Flg*<sup>-/-</sup> mice. \**P* < .05 and \*\**P* < .01.

solubilized in water did not penetrate either wild-type or *Flg*<sup>-/-</sup> SC (Fig 6, **A** and **B**), indicating that the SC remained hydrophobic. It is of note that lipid composition was aberrant in *Flg*<sup>-/-</sup> SC, whereas free fatty acid levels remained normal, and levels of ceramide and cholesterol were increased (see the Methods section and Fig E4 in this article's Online Repository at www.jacionline.org). It is possible that aberrant lipid composition, as well as SC fragility, might have direct or indirect effects on the penetration of certain materials by affecting SC hydrophobicity.

Barrier disruption and continuous percutaneous exposure to allergens presumably initiate and drive AD. *Flg*<sup>-/-</sup> SC allowed the penetration of both hapten and protein antigens, which was followed by exaggerated immune responses. The *ft/ma* mice spontaneously have itchy skin lesions,<sup>14,15</sup> thus providing an attractive model for AD research. However, we showed that they do not completely lack filaggrin. This, together with the presence of the matted mutation, means that it is difficult to explore precise mechanisms of skin sensitization and dermatitis progression at the molecular level with *ft/ma* mice. Use of *Flg*<sup>-/-</sup> mice revealed

that filaggrin was required for proper barrier formation *in vivo* and that its loss resulted in enhanced percutaneous cellular and humoral immune responses, which are important steps in the early phase of AD pathogenesis.

The insolubility of the SC has hampered progress in understanding its biology. Genetic ablation of relevant molecules *in vivo* is thus far the only method to overcome this issue. By generating *Flg*<sup>-/-</sup> mice, we demonstrated that filaggrin is necessary for proper barrier formation *in vivo*, with filaggrin deficiency leading to enhanced penetration of antigens and subsequent sensitization. Loss of or functional abnormalities in filaggrin is important in the early phase of AD development. Other environmental or genetic factors can be examined in these mice to further dissect SC biology *in vivo* and to explore other factors that contribute to prolonged and progressive dermatitis in the context of AD.

We thank Dr Akemi Ishida-Yamamoto and Dr Hiroyuki Sasaki for technical advice and technical support on TEM, Dr Tadafumi Kawamoto for technical assistance with the Kawamoto film method, and Mr Taizen Morishita for the

amino acid analysis. We also thank Ms Minae Suzuki for the preparation of frozen sections and Ms Hiromi Itoh for excellent animal care. Scanning electron microscopic analysis was a courtesy of Hitachi High-Technologies Corporation.

**Clinical implications: The newly generated *Flg*<sup>-/-</sup> mice enabled the evaluation of filaggrin function *in vivo* and might be a highly useful tool for studying the epidermal barrier at the molecular level.**

## REFERENCES

- Segre JA. Epidermal barrier formation and recovery in skin disorders. *J Clin Invest* 2006;116:1150-8.
- Elias PM, Schmuth M. Abnormal skin barrier in the etiopathogenesis of atopic dermatitis. *Curr Opin Allergy Clin Immunol* 2009;9:437-46.
- Steinert PM, Cantieri JS, Teller DC, Lonsdale-Eccles JD, Dale BA. Characterization of a class of cationic proteins that specifically interact with intermediate filaments. *Proc Natl Acad Sci U S A* 1981;78:4097-101.
- Sandilands A, Sutherland C, Irvine AD, McLean WH. Filaggrin in the frontline: role in skin barrier function and disease. *J Cell Sci* 2009;122:1285-94.
- Dale BA, Holbrook KA, Steinert PM. Assembly of stratum corneum basic protein and keratin filaments in macrofibrils. *Nature* 1978;276:729-31.
- Dale BA, Resing KA, Lonsdale-Eccles JD. Filaggrin: a keratin filament associated protein. *Ann N Y Acad Sci* 1985;455:330-42.
- Kamata Y, Taniguchi A, Yamamoto M, Nomura J, Ishihara K, Takahara H, et al. Neutral cysteine protease bleomycin hydrolase is essential for the breakdown of deiminated filaggrin into amino acids. *J Biol Chem* 2009;284:12829-36.
- Rawlings AV, Harding CR. Moisturization and skin barrier function. *Dermatol Ther* 2004;17(suppl 1):43-8.
- Smith FJ, Irvine AD, Terron-Kwiatkowski A, Sandilands A, Campbell LE, Zhao Y, et al. Loss-of-function mutations in the gene encoding filaggrin cause ichthyosis vulgaris. *Nat Genet* 2006;38:337-42.
- Irvine AD. Fleshing out filaggrin phenotypes. *J Invest Dermatol* 2007;127:504-7.
- Palmer CN, Irvine AD, Terron-Kwiatkowski A, Zhao Y, Liao H, Lee SP, et al. Common loss-of-function variants of the epidermal barrier protein filaggrin are a major predisposing factor for atopic dermatitis. *Nat Genet* 2006;38:441-6.
- Bieber T. Atopic dermatitis. *N Engl J Med* 2008;358:1483-94.
- McGrath JA, Uitto J. The filaggrin story: novel insights into skin-barrier function and disease. *Trends Mol Med* 2008;14:20-7.
- Moniaga CS, Egawa G, Kawasaki H, Hara-Chikuma M, Honda T, Tanizaki H, et al. Flaky tail mouse denotes human atopic dermatitis in the steady state and by topical application with *Dermaphagoides pteronyssinus* extract. *Am J Pathol* 2010;176:2385-93.
- Oyoshi MK, Murphy GF, Geha RS. Filaggrin-deficient mice exhibit TH17-dominated skin inflammation and permissiveness to epicutaneous sensitization with protein antigen. *J Allergy Clin Immunol* 2009;124:485-93, e1.
- Fallon PG, Sasaki T, Sandilands A, Campbell LE, Saunders SP, Mangan NE, et al. A homozygous frameshift mutation in the mouse *Flg* gene facilitates enhanced percutaneous allergen priming. *Nat Genet* 2009;41:602-8.
- Scharschmidt TC, Man MQ, Hatano Y, Crumrine D, Gunathilake R, Sundberg JP, et al. Filaggrin deficiency confers a paracellular barrier abnormality that reduces inflammatory thresholds to irritants and haptens. *J Allergy Clin Immunol* 2009;124:496-506, e1-6.
- Jarrett A, Spearman RI. The keratin defect and hair-cycle of a new mutant (matted) in the house-mouse. *J Embryol Exp Morphol* 1957;5:103-10.
- Lane PW. Two new mutations in linkage group XVI of the house mouse. Flaky tail and varitint-waddler-J. *J Hered* 1972;63:135-40.
- Searle A, Spearman R. "Matted," a new hair-mutant in the house-mouse: genetics and morphology. *J Embryol Exp Morphol* 1957;5:93-102.
- Kezic S, Kemperman PM, Koster ES, de Jongh CM, Thio HB, Campbell LE, et al. Loss-of-function mutations in the filaggrin gene lead to reduced level of natural moisturizing factor in the stratum corneum. *J Invest Dermatol* 2008;128:2117-9.
- O'Regan GM, Kemperman PM, Sandilands A, Chen H, Campbell LE, Kroboth K, et al. Raman profiles of the stratum corneum define 3 filaggrin genotype-determined atopic dermatitis endophenotypes. *J Allergy Clin Immunol* 2010;126:574-580.e1.
- Proksch E, Folster-Holst R, Jensen JM. Skin barrier function, epidermal proliferation and differentiation in eczema. *J Dermatol Sci* 2006;43:159-69.
- Fluhr JW, Elias PM, Man MQ, Hupe M, Selden C, Sundberg JP, et al. Is the filaggrin-histidine-urocanic acid pathway essential for stratum corneum acidification? *J Invest Dermatol* 2010;130:2141-4.
- Brody I. The keratinization of epidermal cells of normal guinea pig skin as revealed by electron microscopy. *J Ultrastruct Res* 1959;2:482-511.
- Brody I. The ultrastructure of the tonofibrils in the keratinization process of normal human epidermis. *J Ultrastruct Res* 1960;4:264-97.
- Norlen L, Al-Amoudi A. Stratum corneum keratin structure, function, and formation: the cubic rod-packing and membrane templating model. *J Invest Dermatol* 2004;123:715-32.
- Kawamoto T. Use of a new adhesive film for the preparation of multi-purpose fresh-frozen sections from hard tissues, whole-animals, insects and plants. *Arch Histol Cytol* 2003;66:123-43.
- Kubo A, Nagao K, Yokouchi M, Sasaki H, Amagai M. External antigen uptake by Langerhans cells with reorganization of epidermal tight junction barriers. *J Exp Med* 2009;206:2937-46.
- Ouchi T, Kubo A, Yokouchi M, Adachi T, Kobayashi T, Kitashima DY, et al. Langerhans cell antigen capture through tight junctions confers preemptive immunity in experimental staphylococcal scalded skin syndrome. *J Exp Med* 2011;208:2607-13.
- Nagao K, Ginhoux F, Leitner WW, Motegi S, Bennett CL, Clausen BE, et al. Murine epidermal Langerhans cells and langerin-expressing dermal dendritic cells are unrelated and exhibit distinct functions. *Proc Natl Acad Sci U S A* 2009;106:3312-7.
- Larson RP, Zimmerli SC, Comeau MR, Itano A, Omori M, Iseki M, et al. Dibutyl phthalate-induced thymic stromal lymphopoietin is required for Th2 contact hypersensitivity responses. *J Immunol* 2010;184:2974-84.
- Nemoto-Hasebe I, Akiyama M, Nomura T, Sandilands A, McLean WH, Shimizu H. Clinical severity correlates with impaired barrier in filaggrin-related eczema. *J Invest Dermatol* 2009;129:682-9.
- Manabe M, Sanchez M, Sun TT, Dale BA. Interaction of filaggrin with keratin filaments during advanced stages of normal human epidermal differentiation and in ichthyosis vulgaris. *Differentiation* 1991;48:43-50.
- Sybert VP, Dale BA, Holbrook KA. Ichthyosis vulgaris: identification of a defect in synthesis of filaggrin correlated with an absence of keratohyaline granules. *J Invest Dermatol* 1985;84:191-4.
- Gruber R, Elias PM, Crumrine D, Lin TK, Brandner JM, Hachem JP, et al. Filaggrin genotype in ichthyosis vulgaris predicts abnormalities in epidermal structure and function. *Am J Pathol* 2011;178:2252-63.

## METHODS

### Generation of *Flg*<sup>-/-</sup> mice

*Flg*<sup>-/-</sup> mice were generated by means of homologous recombination. The murine filaggrin gene (*Flg*), which is located on chromosome 3, consists of 3 exons and shares unique characteristics with its human counterpart. Exon 1 consists of 5' UTR sequences, exon 2 contains the translation start site, and the unusually large exon 3 encodes filaggrin repeats that are almost identical with each other, flanked by a 5'-specific sequence encoding the S-100 domain and a 3'-specific sequence followed by a 3'-UTR (Fig E1, A). Large open reading frames and repetitive sequences complicated the strategy by which the genes were targeted.

We designed the targeting vector to remove both the start codon located in exon 2 and in-frame ATG sequences located at the 5'-end of exon 3, which excluded all in-frame ATG sequences in *Flg*. The 3' short homology arm was designed to include 5'-specific *Flg* sequences and part of the first filaggrin repeat (Fig E1, A) to minimize the possibility of unexpected recombination within the filaggrin repeats. Electroporation of the targeting vector into C57BL/6 ES cells did not yield any appropriately recombined ES cells. Using BA1 hybrid (C57BL/6 × 129/SvEv background) ES cells, we successfully obtained an ES cell clone named 824 in which homologous recombination between the targeting vector and *Flg* at the side of the long homology arm was confirmed by means of Southern blotting of *Bam*HI-digested genomic DNA by using a probe specific for the outside of the long homology arm (Fig E1, A, blue; wild-type = 11.8 kb; F1 hetero = 9.1 kb; data not shown). ES cell clone 824 was injected into C57BL/6 blastocysts, and chimeric mice were obtained. One of the chimeric mice was crossed with a C57BL/6 wild-type mouse. Southern blotting analysis of *Bam*HI-digested genomic DNA of F1 generation mice with the above probe successfully identified F1 hetero mice (Fig E1, B). To confirm successful recombination at the side of the short homology arm and integration of only 1 copy of the targeting vector, we performed Southern blotting with a probe specific for the 5'-specific *Flg* sequence located within the short homology arm. When genomic DNA from wild-type C57BL/6 and 129/SvEv mice was digested by *Msc*I and analyzed by means of Southern blotting with this probe (Fig E1, A, red), a 6-kb band and a 10-kb band were detected, respectively, indicating the existence of a polymorphism within the filaggrin repeats (Fig E1, C). Because the amount of genomic DNA excluded by means of gene targeting was almost the same as the size of the neomycin cassette of the targeting vector, successfully targeted mice were predicted to produce same-sized bands as wild-type mice (Fig E1, A). Although only a 6-kb band was detected in F1 hetero mice, both 6- and 10-kb bands were detected in their wild-type littermates, indicating that the C57BL/6 *Flg* allele had been targeted (Fig E1, C). These results also indicated the integration of a single copy of the targeting vector and the absence of unexpected homologous recombination between the short homology arm and filaggrin repeat sequences. Mice were backcrossed to C57BL/6 and BALB/c backgrounds to minimize phenotypic variation, especially in the context of immune response analyses.

### Southern blotting

Genomic DNA from ES cells, mice tails, and hepatics was digested with the appropriate restriction enzymes. DNA fragments were separated by using 0.7% agarose gel electrophoresis, transferred to GeneScreen Plus membranes (NEN Life Science Products), and hybridized at 65°C with phosphorous 32-labeled insert cDNA.

### Antibodies

Antibodies against filaggrin (Covance, Berkeley, Calif), involucrin, loricrin, keratin 1 (all Abcam, Cambridge, Mass), and actin (Santa Cruz Biotechnology, Santa Cruz, Calif) were used for immunoblotting and immunohistochemistry.

### Immunoblotting

Urea/Tris extracts were prepared from 5-day-old mice, as described previously.<sup>E1</sup> Protein samples were fractionated by means of SDS-PAGE and transferred to Immobilon-P membranes (Millipore, Bedford, Mass).

Membranes were treated with primary antibodies. Bound primary antibody was detected with an alkaline phosphatase-conjugated secondary antibody (Zymax, San Francisco, Calif).

### Histologic analysis

Skin specimens were fixed in 10% buffered formalin and embedded in paraffin. For immunohistochemical analysis, primary antibodies were detected with an ImmPRESS Reagent kit (Vector Laboratories, Burlingame, Calif). For frozen sections, tissues were embedded in Tissue-Tek OCT compound (Sakura Finetechnical, Tokyo, Japan) in a liquid nitrogen-cooled isopentane bath. Safranin staining was performed to enhance visualization of SC layers, as described previously.<sup>E2</sup>

### Negative replica imaging

Negative replica images of the dorsal skin surface in neonatal mice were obtained by using SILFLO (Flexico Developments Ltd, Potters Bar, United Kingdom), a silicon-based gum material, and were analyzed with laser profilometry (Primos; GFMesstechnik GmbH, Teltow, Germany).

### Biophysical skin measurements

For the analysis of amino acid content, SC samples were obtained from 1.5 × 2.0-cm<sup>2</sup> regions of dorsal skin in 4-day-old neonatal mice through 6 rounds of TS (Scotch tape; 3M, St Paul, Minn). The SC was detached from the tape with toluene. After the solvent was evaporated, amino acids were extracted with 10% sulphosalicylic acid solution and subjected to amino acid analysis with an amino acid analyzer (Hitachi, Tokyo, Japan).

NMF, lipid, and water concentration profiles in murine SC were analyzed by using *in vivo* confocal Raman microscopy (Model 3510 Skin Composition Analyzer; River Diagnostics, Rotterdam, The Netherlands) with previously described methods.<sup>E3</sup> Molecule concentration profiles in the abdominal SC of 2- to 5-day-old neonatal mice were measured at intervals of 2 μm to a depth of 8 μm. Raman spectra were recorded in the spectral region at 400 to 1800 cm<sup>-1</sup> with a 785-nm laser for the measurement of NMF and lipid components and at 1500 to 3800 cm<sup>-1</sup> with a 671-nm laser for the measurement of water. NMFs were measured as the sum of the spectra for the dominant constituents (serine, glycine, pyrrolidone-5-carboxylic acid, proline, ornithine, histidine, and alanine) by using the signal intensity of the Raman spectrum for keratin as the reference value. The water/protein ratio was calculated as the ratio between the Raman signal intensity of water (caused by OH-stretching vibrations) integrated from 3350 to 3550 cm<sup>-1</sup> and that of protein (caused by CH<sub>3</sub>-stretching vibrations) integrated from 2910 to 2965 cm<sup>-1</sup> to determine SC water concentrations.

SC lipid contents of lipid extracts isolated from SC sheets from the same area were measured. Epidermal sheets were obtained from 10 mmol/L dithiothreitol-treated skin and were then incubated for 10 minutes at 37°C in 0.25% trypsin solution. After incubation, samples were gently vortexed to remove residual nucleated cells and washed with PBS 3 times. SC lipids were extracted from these SC sheets and analyzed by using high-performance thin-layer chromatography, as described previously.<sup>E4</sup>

Measurements of SC conductance, TEWL, and SC surface pH were performed at room temperature (22°C-26°C) and 40% to 60% humidity. SC hydration was evaluated by analyzing skin electrical impedance<sup>E5</sup> with a Corneometer ASA-M2 (Asahi Biomed, Yokohama, Japan).<sup>E6</sup> TEWL was measured with a VAPOSCAN AS-VT100RS machine (Asahi Biomed). SC surface pH was evaluated with the skin pH meter PH 905 (Courage & Khazaka, Cologne, Germany). All data are presented as the median of 3 repeated recordings.

### Electron microscopy

For low-vacuum scanning electron microscopic analysis, feet, tails, and dorsal and abdominal skin were harvested from P5 neonatal mice and fixed in glutaraldehyde. After dehydration in tert-butyl alcohol, samples were observed with a low-vacuum scanning electron microscope (S-3400N; Hitachi High-Tech, Tokyo, Japan).

Skin samples were fixed with 2% glutaraldehyde and 1% osmium tetroxide and processed for conventional TEM. For visualization of SC structures, skin

samples were fixed with half-strength Karnovsky fixative and then with 0.2% ruthenium tetroxide and 0.5% potassium ferrocyanide in 0.1 mol/L sodium cacodylate (pH 6.8).<sup>E7</sup>

### Fragility assay

The dorsal skin of P4 neonatal mice was repeatedly tape stripped at the same sites with Cryofilm Type 2C (Leica Microsystems, Tokyo, Japan) to assess the detachment of cornified layers under mechanical stress. The amount of detached cornified material on the tape was evaluated by using a modified form of the DIA described previously.<sup>E8</sup> Briefly, light transmission images of cornified materials on the tape were acquired by using an Axio Observer Z1 microscope (Carl Zeiss, Oberkochen, Germany) equipped with a  $\times 5$  objective and were analyzed with Image Pro Plus version 6.2 software (Media Cybernetics, Inc, Silver Spring, Md). Within the observed area, the grayscale pixel distribution ranging from 0 (black) to 255 (white) was determined. The desquamation index was calculated as follows:

$$\text{Desquamation index} = \sum_{n=1}^{255} A_n \times n,$$

where  $A_n$  denotes the number of pixels at gray level  $n$ . Calculation of the desquamation index is based on the assumption that the whiteness of the scales is roughly proportional to their thickness.<sup>E9</sup>

### Permeability assay

A saturated solution of calcein (Bis[N,N-bis(carboxymethyl)aminomethyl] fluorescein; Sigma-Aldrich) or calcein solution including calcein encapsulated in liposomes prepared from Presome CSII-101 (Nippon Fine Chemical, Osaka, Japan).<sup>E10</sup> was topically applied to the tails of 6- to 8-week-old mice for 3 hours. The tails were then removed and rapidly freeze embedded.

The Kawamoto film method was used, with modifications, for accurate evaluation because it prevents diffusion of fluorescence and preserves tissue components during sample preparation.<sup>E11</sup> Cryofilm was fastened to the cut surfaces of the samples to allow nondamaged SC to be visualized, and freeze sectioning was performed. Permeability was evaluated by using confocal microscopy without fixing to prevent the oozing of fluorescent substances.

### Serum antibody analysis

OVA-specific antibody levels were measured by using ELISA. For the analysis of OVA-specific IgE levels, 96-well MaxiSorp ELISA plates (Nunc, Roskilde, Denmark) were coated with capture IgE antibody by using a murine IgE quantitative ELISA kit (Bethyl Laboratories, Montgomery, Tex) for 60 minutes and then blocked with 3% skim milk in PBS for 60 minutes. After blocking, serum samples (50  $\mu$ L) diluted in Can Get Signal Solution 1 (TOYOBO, Tokyo, Japan) to an appropriate concentration were added to

appropriate wells, and the plate was incubated for 60 minutes. After washing, OVA (1.5  $\mu$ g/mL in Can Get Signal Solution 1) was added to each well, and the plate was incubated for 60 minutes. Horseradish peroxidase-conjugated anti-OVA (Rockland, Gilbertsville, Pa; diluted 1:10,000 in Can Get Signal Solution 2) was added for 60 minutes. TMB substrate was applied, and the absorbance at 450 nm was measured.

For the analysis of OVA-specific IgG<sub>1</sub> levels, plates were coated with OVA (10  $\mu$ g/mL in PBS) at 4°C overnight. After blocking, 500-fold diluted sera were added to appropriate wells, and the plate was incubated for 2 hours. Horseradish peroxidase-conjugated anti-mouse IgG<sub>1</sub> (100  $\mu$ L, dilution 1:10,000, Bethyl Laboratories) was applied for 2 hours to conjugate the antigen-antibody complex. TMB substrate was applied, and the absorbance at 450 nm was measured.

### REFERENCES

- E1. Presland RB, Boggess D, Lewis SP, Hull C, Fleckman P, Sundberg JP. Loss of normal profilaggrin and flaggrin in flaky tail (*ft/ft*) mice: an animal model for the flaggrin-deficient skin disease ichthyosis vulgaris. *J Invest Dermatol* 2000; 115:1072-81.
- E2. Ya-Xian Z, Suetake T, Tagami H. Number of cell layers of the stratum corneum in normal skin—relationship to the anatomical location on the body, age, sex and physical parameters. *Arch Dermatol Res* 1999;291:555-9.
- E3. Caspers PJ, Lucassen GW, Carter EA, Bruining HA, Puppels GJ. In vivo confocal Raman microspectroscopy of the skin: noninvasive determination of molecular concentration profiles. *J Invest Dermatol* 2001;116:434-42.
- E4. Weerheim A, Ponc M. Determination of stratum corneum lipid profile by tape stripping in combination with high-performance thin-layer chromatography. *Arch Dermatol Res* 2001;293:191-9.
- E5. Yamamoto Y. Measurement and analysis of skin electrical impedance. *Acta Derm Venereol Suppl (Stockh)* 1994;185:34-8.
- E6. Tomita Y, Akiyama M, Shimizu H. Stratum corneum hydration and flexibility are useful parameters to indicate clinical severity of congenital ichthyosis. *Exp Dermatol* 2005;14:619-24.
- E7. Hou SY, Mitra AK, White SH, Menon GK, Ghadially R, Elias PM. Membrane structures in normal and essential fatty acid-deficient stratum corneum: characterization by ruthenium tetroxide staining and x-ray diffraction. *J Invest Dermatol* 1991;96:215-23.
- E8. Soma Y, Kashima M, Imaizumi A, Takahama H, Kawakami T, Mizoguchi M. Moisturizing effects of topical nicotinamide on atopic dry skin. *Int J Dermatol* 2005;44:197-202.
- E9. El Gammal C, Pagnoni A, Kligman AM, el Gammal S. A model to assess the efficacy of moisturizers—the quantification of soap-induced xerosis by image analysis of adhesive-coated discs (D-Squames). *Clin Exp Dermatol* 1996;21: 338-43.
- E10. El Maghraby GM, Barry BW, Williams AC. Liposomes and skin: from drug delivery to model membranes. *Eur J Pharm Sci* 2008;34:203-22.
- E11. Kawamoto T. Use of a new adhesive film for the preparation of multi-purpose fresh-frozen sections from hard tissues, whole animals, insects and plants. *Arch Histol Cytol* 2003;66:123-43.

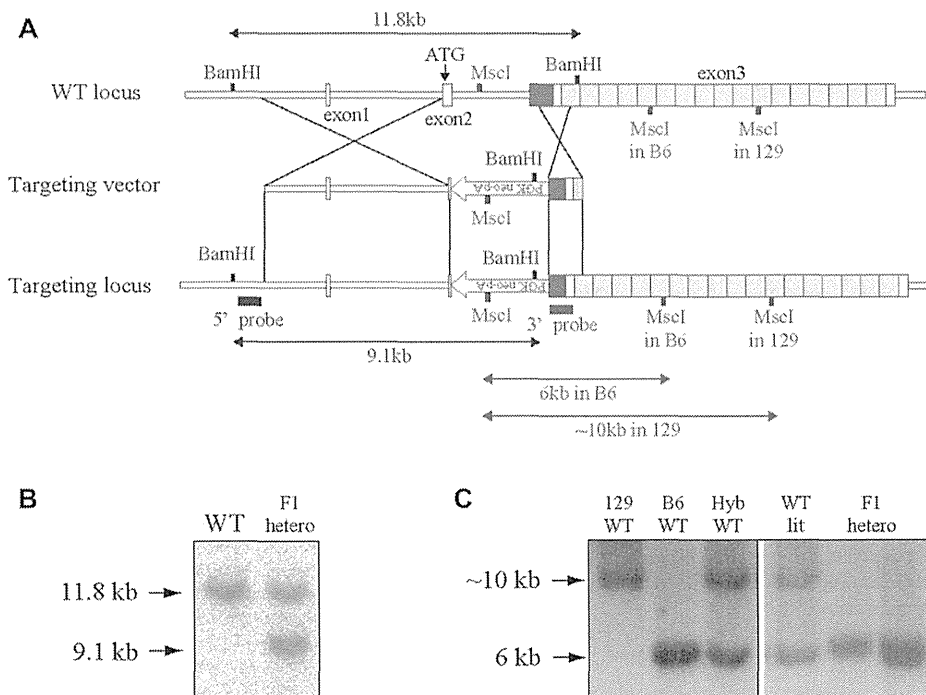


**FIG E1.** A, Partial restriction enzyme maps and schematic representation of the strategy used to ablate *Fig* expression in mice. B and C, Southern blot analyses with *Bam*HI-digested (Fig E1, B) and *Msc*I-digested (Fig E1, C) genomic DNA were performed to confirm the successful recombination at the sides of the long (Fig E1, B) and short (Fig E1, C) homology arms, respectively. WT, Wild-type.

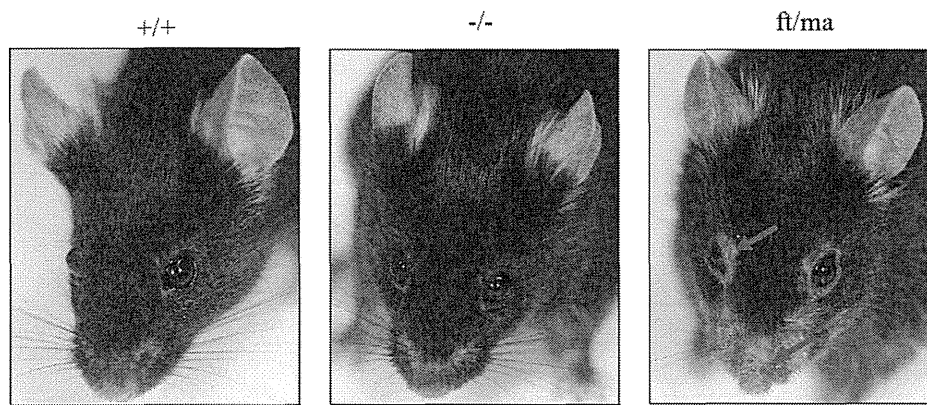


**FIG E2.** Clinical photographs of 12- to 15-week-old wild-type (+/+), *Flg*<sup>-/-</sup> (-/-), and *ft/ma* mice under SPF conditions. Whereas *ft/ma* mice had dermatitis (*arrows*) spontaneously, *Flg*<sup>-/-</sup> mice did not have any cutaneous manifestation.

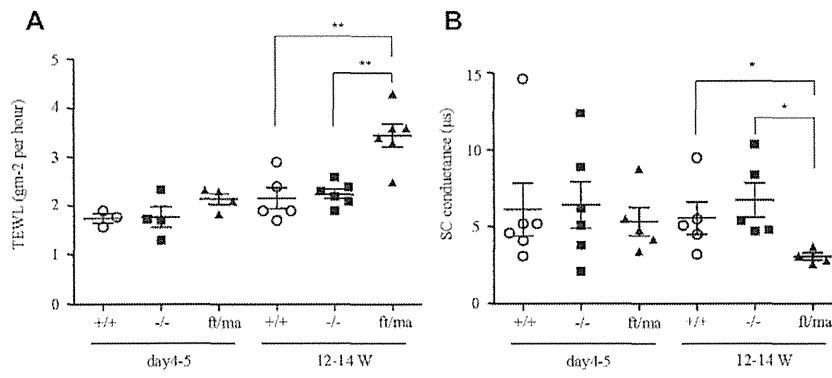


**FIG E3.** Comparison of TEWL (A) and SC hydration (B) between P4 and P5 and 12- to 14-week-old wild-type (+/+), *Flg*<sup>-/-</sup> (-/-), and *ft/ma* mice in a steady state under normal unmanipulated housing conditions. At 12 to 14 weeks, the *ft/ma* mice used in this study had spontaneous dermatitis. \**P* < .05 and \*\**P* < .01.



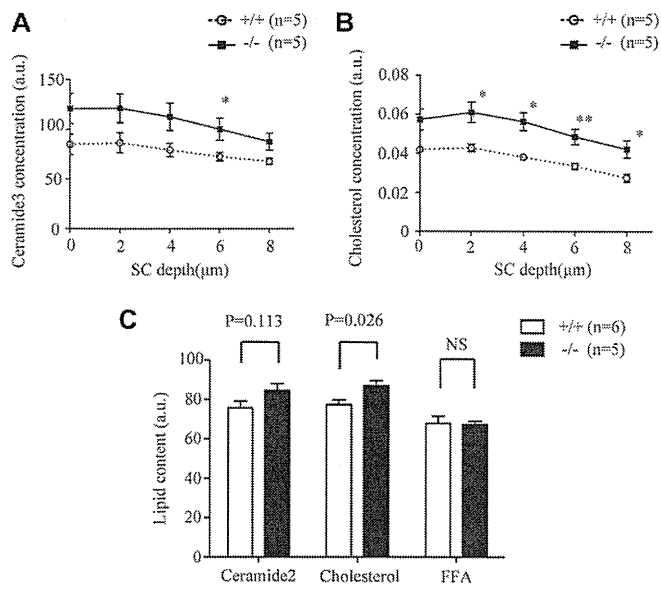


**FIG E4.** Comparison of SC lipid contents between neonatal wild-type (+/+) and *Flg*<sup>-/-</sup> (-/-) mice. **A** and **B**, Dorsal skin ceramide 3 (Fig E4, A) and cholesterol (Fig E4, B) profiles were measured by using *in vivo* confocal Raman microspectroscopy. **C**, Analysis of lipid extracts isolated from SC sheets. FFA, Free fatty acids; NS, not significant. \**P* < .05 and \*\**P* < .01.

創薬基盤推進研究事業

悪性中皮腫のヒト化CD26抗体療法の確立及び化学療法剤の  
有効性評価に有用な新規疾患関連バイオマーカーの開発

平成24年度～26年度

総合研究報告書

平成27年3月31日発行

発行：研究代表者 森本 幾夫

〒113-8421 東京都文京区本郷2-1-1

順天堂大学大学院医学研究科 免疫病・がん先端治療学講座

TEL : 03-3868-2310

